GS-15

STRUCTURAL ANALYSIS AND GOLD METALLOGENY OF THE FARLEY LAKE GOLD DEPOSIT, LYNN LAKE GREENSTONE BELT (NTS 64C/16)

by C.J. Beaumont-Smith, D.R. Lentz[1] and E.A. Tweed[2]

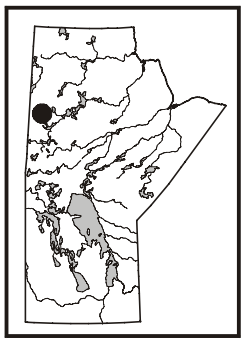

Beaumont-Smith, C.J., Lentz, D.R. and Tweed, E.A. 2000: Structural analysis and gold metallogeny of the Farley Lake gold deposit, Lynn Lake greenstone belt (NTS 64C/16); *in* Report of Activities 2000, Manitoba Industry, Trade and Mines, Manitoba Geological Survey, p. 73-81.

SUMMARY

Preliminary structural and geochemical investigations of the Farley Lake gold deposit have determined that the gold mineralization is the result of emplacement of postdeformational, postplutonic quartz-carbonate-sulphide veins into banded oxide- and silicate-facies iron-formation, and the accompanying sulphidization of the iron-formation. The high-grade quartz-carbonate-sulphide veins were emplaced along preexisting, shallowly southwest-dipping joints and subvertical D_2 faults and shears. The thick sequence of iron-formation and interbedded argillaceous sedimentary rocks that hosts the mineralization has undergone significant D_1 and D_2 fold thickening.

INTRODUCTION

The Farley Lake gold deposit is located in the northern Lynn Lake greenstone belt, approximately 45 km northeast of the town of Lynn Lake (Fig. GS-15-1). The deposit consists of four zones of gold mineralization, the Wendy, South, Southeast and East zones (Richardson and Ostry, 1996), hosted by a thick sequence of banded oxide-, silicate- and sulphide-facies iron-formation (Fedikow, 1995). Production from the Wendy and East open pits between 1996 and 1999 totalled, based on published reserves, 635 000 t of pyrrhotite-associated ore averaging 6.86 g/t Au and 363 000 t of pyrite-associated ore averaging 4.80 g/t Au, respectively (Richardson and Ostry, 1996). The total preproduction resource stood at 1.45 million t grading 3.90 g/t Au (Richardson and Ostry, 1996).

The Farley Lake deposit is hosted by Wasekwan Group (Bateman, 1945) volcanic and sedimentary rocks that constitute the Agassiz Metallotect (Fedikow and Gale, 1982), a stratigraphic succession defined, from top to bottom, by high Mg-Cr basalt (picrite), rhyolitic to dacitic volcanic rocks, argillaceous sedimentary rocks and exhalative sedimentary rocks. The mine sequence is tightly folded (F_1) into an overall upright anticlinal structure. A smaller synclinal inlier of carbonaceous shale, plunging moderately to the west (Peck et al., 1998), occurs in the roof of this larger F_1 feature; the anticline is therefore cored by banded iron-formation. The deposit is unique relative to other gold deposits in the Lynn Lake greenstone belt in that gold mineralization (centimetre- to decimetre-scale quartz-sulphide veins (QSV) hosted in banded iron-formation) is associated with late faults and joints that are discordant with the earlier tectonic fabrics. Other gold deposits, namely the Burnt Timber and MacLellan deposits, are characterized by the emplacement of gold mineralization and associated hydrothermal alteration early in the deformational history, possibly prior to and coincident with fabric development and peak amphibolite-grade regional metamorphism.

Investigations of the gold mineralization at the Farley Lake deposit involved detailed structural analysis of the East pit, including geochemical sampling of mineralization exposed in the pit and selected diamond-drill core. Mining operations in the Wendy pit were suspended in 1998 and the pit is completely flooded, precluding it from structural analysis. Production from the East pit concluded in October of 1999 and the pit is in the process of flooding. Structural analysis of the East pit was initiated in September 1999, with the mapping of the lower production benches. Mapping and sampling of the upper benches and preliminary diamond-drill core study and sampling were completed this summer.

DEPOSIT GEOLOGY

The Farley Lake gold deposit is hosted by a fold-thickened sedimentary succession of thinly layered iron-formation and argillaceous sedimentary rocks located within the core of an east-trending anticline (Fig. GS-15-2; Peck et al., 1998). This sedimentary sequence is overlain

[1] Department of Geology, University of New Brunswick, P.O. Box 4400, Fredericton, New Brunswick E3B 5A3

[2] Department of Earth and Atmospheric Sciences, University of Alberta, Edmonton, Alberta T6G 2E3

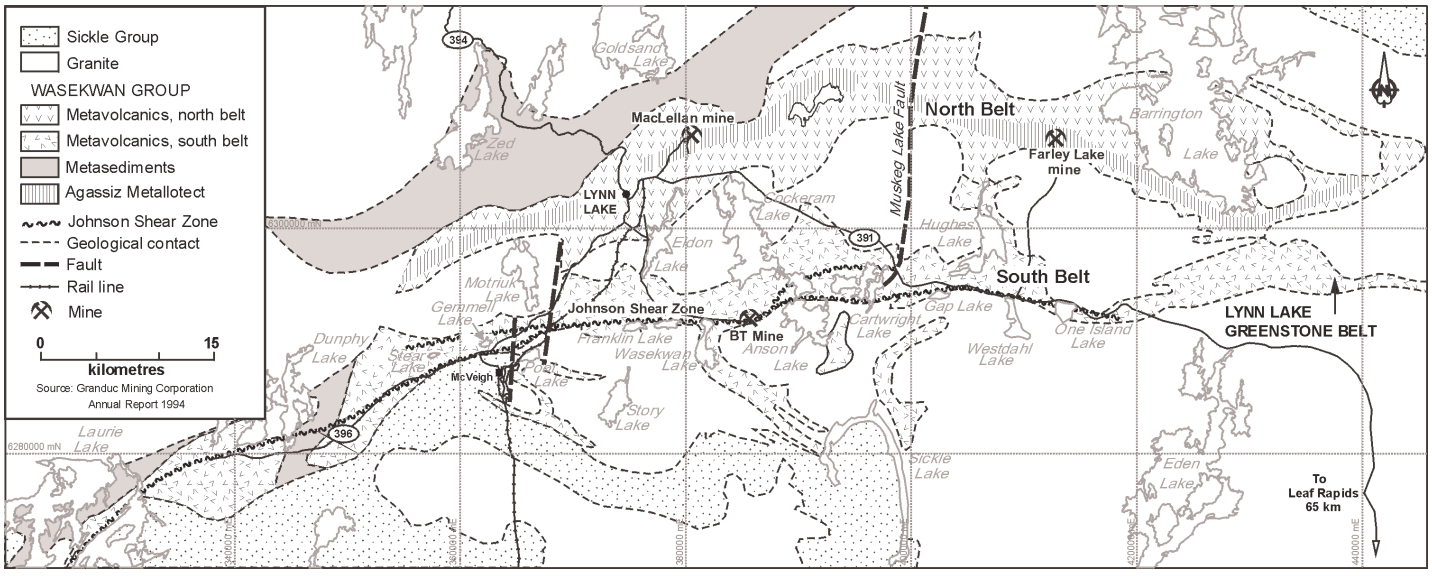

*Figure GS-15-1: General geology of the Lynn Lake greenstone belt and location of the Johnson Shear Zone (*after *Peck et al., 1998).*

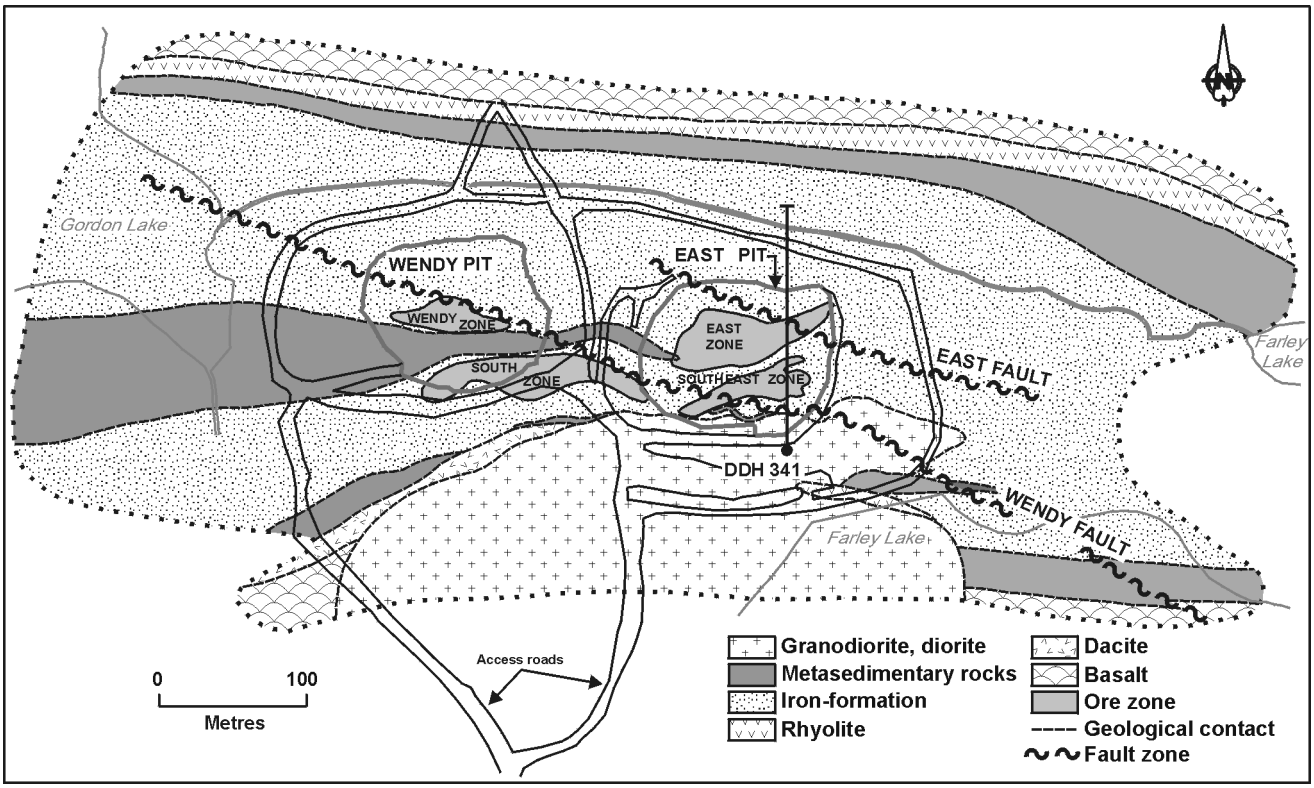

*Figure GS-15-2: Local geology of the Farley Lake deposit (*after *Peck et al., 1998).*

by dacitic (south) and rhyolitic (north) volcanic rocks and high-Mg-Cr basalt (picrite). The southern margin of the deposit has been discordantly intruded by a granodioritic to dioritic pluton of the Pool Lake intrusive suite (Gilbert et al., 1980). The pluton is in direct contact with mineralized iron-formation along the southern edge of the East pit.

The iron-formation unit is approximately 600 m wide and has a strike length in excess of 6 km (Milligan, 1960). It is composed of, in decreasing order of abundance, finely laminated magnetite-chert (oxide facies), magnetite-grunerite-chert (silicate facies) and pyrrhotite-chert (sulphide facies). The oxide facies consists of thin, alternating magnetite and chert laminations of roughly equal proportions. The minor amounts of interlayered carbonate within this facies appears to represent transposed pre- to syn-D_2 veins. The silicate facies is composed of finely laminated chert and beige amphibole (grunerite-anthophyllite)-magnetite layers. This facies probably resulted from an increased hemipelagic component during deposition. The sulphide facies constituted a relatively minor component in the East zone of the deposit, but represents a volumetrically important constituent of the Wendy zone, largely hosting the mineralization (Richardson and Ostry, 1996). Sulphide-facies iron-formation exposed in the lower portions of the East pit comprise thin (1–2 m) interbedded units of finely laminated chert with thin pyrrhotite laminae and abundant, coarsely disseminated pyrrhotite porphyroblasts. The latter form 1 to 2 mm blebs and trains of discontinuously interconnected blebs. Where well foliated, thin pyrrhotite stringers define the foliation. Total pyrrhotite content approaches 40% by volume.

There appears to be a systematic distribution of oxide and silicate iron-formation facies in the East pit. The southern portion of the pit is dominated by oxide facies with minor interbeds of silicate- and sulphide-facies iron-formation. The northern portion of the pit is underlain by silicate-facies iron-formation with only minor oxide facies.

Interbedded with the iron-formation are thin, clastic sedimentary units (approx. 1–2 m average thickness), which locally reach a thickness of 50 m in the core of the regional antiform. These rocks comprise thinly bedded sequences of argillite, chloritic argillite and minor siltstone. Several 10 to 20 cm thick silicate-facies grunerite-garnet iron-formation horizons are tightly fold-intercalated with the thick argillite unit exposed in the west wall of the East pit.

Recrystallization associated with regional lower amphibolite facies metamorphism has resulted in the general coarsening of the constituent mineral phases, the growth of amphibole in the silicate-facies iron-formation, and the development of calc-silicates in local calcareous iron-formation and premetamorphic carbonate veins. The timing of metamorphism is broadly coeval with the third phase of regional deformation (D_3) and postdates the intrusion of the Pool Lake suite. The growth of randomly oriented grunerite porphyroblasts overprints the main S_2 foliation. Locally, the porphyroblasts have a strong S_3-parallel preferred orientation, suggesting that the differences in degree of porphyroblast preferred orientation reflect slight differences in the timing of grunerite growth due to slight changes of bulk rock chemistry.

Intruding the Wasekwan supracrustal succession is a Pool Lake suite granodioritic to dioritic pluton. The pluton is medium grained, generally equigranular and locally well foliated, particularly near the northern contact with the supracrustal sequence. Although commonly referred to as granodioritic, the intrusion seems to have several phases that were recognized during the original drilling program; the outermost phases are tonalitic to dioritic in composition (*see* next section). Trace to several per cent pyrrhotite and pyrite are commonly found with quartz and carbonate veining associated with coincident chloritized, silicified and carbonatized zones. Although locally mineralized with gold-bearing sulphide-quartz (± carbonate±chlorite) veins, there are numerous late fabrics with sulphide-quartz veins and alteration within each of the intrusive phases that are devoid of gold mineralization. The alteration zones, which are locally associated with anomalous gold abundances, are intimately associated with ductile to brittle shearing that seems to overprint a pre-existing ductile foliation defined by the preferred orientation of biotite, amphibole and plagioclase (i.e. peak metamorphic assemblages). In general, the fabric intensity (weak to intense) and alteration increase toward the northern margin of the pluton. Chloritization of the constituent biotite and hornblende, together with sericitization of the feldspar, results in a distinct colour change that seems to coincide with the introduction of quartz and carbonate, as well as pyrite and pyrrhotite. It is uncertain whether there was considerable early-phase

syndeformational metasomatism, especially since the pluton seems to be reversely zoned toward the margin. The relative timing of the granodioritic and tonalitic phase to the dioritic phase is uncertain. The S_2 foliation seems most intense in the outermost zones of the intrusion; there is minimal fabric within the granodioritic phase, even though there is a high percentage of ferromagnesian silicates present (25%). Nonetheless, the first-phase intrusions predate the main (F_2) folding event, although they are discordant with the folded stratigraphy. This indicates that subsequent deformation, coincident with peak amphibolite-grade metamorphism, followed their intrusion.

GRANODIORITIC TO DIORITIC INTRUSION

In order to ascertain whether the compositional change from the granodiorite to the intensely foliated intrusive margin is associated with a specific episode of hydrothermal alteration or is related to a primary compositional effect, six drill-core samples were taken from available core (diamond-drill hole DDH 341) that was drilled from south to north into the southeastern Farley Lake zone (East pit area). The six-sample profile has an increase in ferromagnesian phases (biotite±amphibole), in part retrograded to hydrothermal biotite, then chlorite and carbonate, from the weakly altered granodiorite into the diorite along the northern contact. Petrographically, the intrusive phases obviously exhibit more intense hydrothermal alteration of the lower temperature variety (Mg-chlorite–carbonate–sulphide) approaching the northern contact. However, granodioritic phases exhibit considerable interstitial biotitic alteration, which seems to have replaced an earlier hornblende- and biotite-bearing granodioritic assemblage. The secondary biotite seems to have a deeper reddish hue than the green igneous biotite. Titanite seems to have been formed as a result of the selective ferromagnesian replacement processes, although coupled with plagioclase alteration (anorthite replacement). The gold-enriched sample (595 ppb Au at 152.4 m [500 ft.] in DDH 341) has intergrown Mg-rich chlorite and carbonate replacing reddish biotite. Pyrrhotite with very minor chalcopyrite occurs in the groundmass with the secondary assemblages, although it is unclear if it is associated with chlorite-carbonate or the hydrothermal biotite. The presence of chalcopyrite in the gold-bearing section is surprising, considering the sample only contained 85 ppm Cu. Based on the original drill log, the altered diorite has an apparent width of approximately 18.3 m (60 ft.) or a 5.2 m (17 ft.) true width. The most intensely altered sample (103.9 m [675 ft.] in DDH 341) contained minor remnant clinopyroxene replaced by an Fe-Mg amphibole (fine to coarse grained), which was in turn partially replaced by and intergrown with Mg-chlorite. The amphibole has a weak preferred orientation. Rutile is secondary after ilmenite. There are several late carbonate veinlets in this sample.

These sample cores were crushed and pulverized in a soft-iron swing mill by the Manitoba Geological Survey and analyzed for major and trace elements, by x-ray fluorescence spectroscopy, instrumental neutron activation analysis and inductively coupled plasma–mass and optical emission spectroscopy, at Activation Laboratories Ltd., Ancaster, Ontario (Table GS-15-1). For duplicate elements, preference was given to techniques not involving dissolution of samples.

Figures GS-15-3 and -4 are variation diagrams illustrating the major-element composition of samples across the profile. As can be seen in Table GS-15-1, there is a consistent decrease in SiO_2 from the core toward the outer margin of the intrusion, consistent with petrographic observations. The Al_2O_3 content decreases slightly from 15.76 to 15.35 wt % with decreasing SiO_2, but then drops off to 8 wt % in the intensely altered (amphibolitized and chloritized) zone near the intrusion margin. If this is a diorite, it is possible to have lower Al_2O_3 contents with higher $Fe_2O_{3\ tot}$ and MgO (32.1 and 9.3 wt %, respectively) at the margin (Fig. GS-15-3b, -3c). The K_2O, Na_2O and CaO contents decrease markedly toward the margin as well (Fig. GS-15-3d, -3e, -3f), which is a function of both primary composition and alteration. The increase in ferromagnesian components at the expense of alkali and alkali-earth elements, including Rb, Ba and Sr, and decreased SiO_2 content are consistent with increasing amphibolitization (?cummingtonite) and chloritization toward the outer margin. The original drill logs noted that these rocks were granodioritic, tonalitic and dioritic in mineralogy, based on textures, many of which were relict. Therefore it is difficult to ascertain whether the more mafic looking rocks, which have greater fabric development and more intense alteration, are actually tonalitic and dioritic in composition. It is possible to test this using immobile elements and their ratios.

Figure GS-15-4a illustrates consistently increasing TiO_2 with decreasing SiO_2. This cannot be related to mass changes, as it is opposite to what would be expected based on the decrease in Al_2O_3 (8 wt %). Also, the TiO_2 co-varies strongly with Sc and V, consistent with an iron tholeiitic composition for the diorite, whereas the other granodioritic and tonalitic samples have a more obvious calc-alkalic signature. There is a decrease in P_2O_5, S, Ni (Fig. GS-15-4b, -4c, -4d), Co and Cr at the outer margin relative to the less altered tonalitic and granodioritic phases of the intrusion. The primitive-mantle–normalized spider diagram (Fig. GS-15-5) for these samples shows that the profiles for the granodiorite and tonalite are similar, although the dioritic sample is notably lower in incompatible elements, except the heavy rare-earth elements (HREE), and higher in TiO_2 (Sc, V), as mentioned earlier. Therefore the light rare-earth element (LREE)/HREE profile of the diorite is notably flatter, typical of a tholeiitic parentage, than for the calc-alkaline samples. Similarly, immobile-element ratios (Fig. GS-15-6a) illustrate that the dioritic sample has a typical tholeiitic signature (Zr/Y = 3), whereas the other samples have values between tholeiitic and calc-alkalic compositions. The Zr/TiO_2 ratio is also consistent with a gabbroic to dioritic composition. All samples plot in the I-type granitoid (volcanic-arc–related) field using the Nb-Y discrimination diagram (Fig. GS-15-6b; Pearce et al., 1984), consistent with their generally aluminous composition. The Th-Zr-Nb discrimination diagram (Fig. GS-15-6c; Wood et al., 1979) shows that the granodioritic and tonalitic samples are of volcanic-arc affinity, whereas the dioritic sample has an enriched mid-ocean ridge basalt (MORB) to within-plate association, which is consistent with the Fe, Mg and TiO_2 contents. The Zr versus Ga/Al contents of these samples (Fig. GS-15-6d; Whalen et al., 1987) indicate an arc signature for the granodiorite and tonalite, although the diorite falls into the anorogenic field, which fits with the tholeiitic (proto-arc or rift-related) interpretation, but not with the Nb/Y ratio, which is much less than 0.7 (*see* Winchester and Floyd, 1977). Based on textural and compositional considerations, it is probable that the diorite is an earlier intrusive phase that was followed by the main volcanic-arc–associated tonalite and granodiorite.

It is also notable that the sample enriched in gold (596 ppb) is associated with high sulphur, although it is evident from the logs and gold assays that this is not always the case. Also, the one anomalous gold sample has low As, Sb, Mo and W. Interestingly, Fedikow (1995) indicated that the gold was not associated with some of the typical indicator elements at the Wendy zone. The sample with the highest gold content is not associated with the most altered (chloritic) sample.

STRUCTURAL ANALYSIS

A major objective of this study is to determine the timing of mineralization relative to alteration, deformation, metamorphism and plutonism in the area. Therefore, an understanding of the structural history of the deposit is critical. Detailed structural analysis of the East pit has delineated four generations of folds (F_1–F_4). The geometry and distribution of the iron-formation appear to be largely controlled by F_1 and F_2 folds, with overprinting by the two younger folding events producing minor redistribution of the older fabric elements. Mesoscopic F_1 folds are rare and are generally recognized as isoclinal, commonly intrafolial folds overprinted by S_2 or refolded by upright, tight, F_2 chevron folds (Fig. GS-15-7). The F_2 folds plunge steeply to the east and are dominantly Z-asymmetrical. A ubiquitous S_2 axial-planar foliation

Table GS-15-1: Analytical data for drillcore samples from the Pool Lake suite granodioritic to dioritic pluton, southeastern Farley Lake zone.

	Sample number (and rock type)					
	DDH341-100 (granodiorite)	**DDH341-300 (granodiorite)**	**DDH341-500 (tonalite)**	**DDH341-515 (tonalite)**	**DDH341-580 (tonalite)**	**DDH341-675 (diorite)**
Major elements (wt %):						
SiO_2	56.51	55.87	53.92	50.34	45.91	40.16
Al_2O_3	15.76	15.88	15.46	15.14	15.35	8
Fe_2O_3	5.93	6.69	6.97	7.8	10.61	32.1
MnO	0.102	0.093	0.117	0.104	0.18	0.361
MgO	3.39	4.05	4.03	5.56	8.8	9.3
CaO	5.86	5.99	6.58	6.39	4.81	2.83
Na_2O	4.93	4.48	3.83	4.31	3.79	0.13
K_2O	1.51	1.89	1.65	2.09	0.31	0.49
TiO_2	0.525	0.588	0.598	0.766	0.819	1.786
P_2O_5	0.34	0.38	0.42	0.5	0.26	0.09
LOI	3.73	2.85	5.15	6.06	8.69	3.9
Total	**98.59**	**98.76**	**98.72**	**99.07**	**99.52**	**99.14**
Trace elements (ppm):						
Nb	11	11	9	11	4	6
Zr	127	128	87	101	65	49
Y	11	12	15	15	22	18
Sr	983	1001	573	781	285	28
Rb	25	34	29	50	3	14
Ba	608	695	697	693	67	93
Ga	17	17	18	17	13	22
S	120	120	1790	95	300	50
Trace elements (ppm):						
Au	2	2	595	27	2	2
As	2.6	3	5.8	11.5	11	43.3
Ba	550	580	660	590	200	210
Co	15	20	23	27	48	71
Cr	80	94	107	143	47	127
Cs	11	12	9	21	2	6
Ni	49	58	57	88	110	28
Sb	0.5	0.4	0.3	0.4	0.1	0.5
Sc	10.2	12	14.2	16.3	28.3	22.4
Ta	0.5	0.5	1.4	0.5	0.5	0.5
Th	3.7	3.1	2.5	2.3	1.1	0.7
U	2.3	1	2.2	1.6	0.9	0.5
W	1	1	7	1	3	1
Zn	70	100	84	100	104	81
La	35	32.6	26.3	27.6	17.1	9.9
Ce	62	60	53	55	34	23
Nd	30	31	31	32	19	16
Sm	6	6.4	6.2	6.7	3.8	4.4
Eu	1.8	1.8	1.8	1.8	1.1	0.7
Tb	0.5	0.8	0.5	0.5	0.5	0.6
Yb	1	1.1	0.9	0.9	2	1
Lu	0.15	0.16	0.15	0.14	0.3	0.14
Trace elements by ICP-OES (ppm):						
Ag	0.3	0.3	0.3	0.3	0.3	0.3
Cd	0.3	0.3	0.3	0.3	0.3	1.6
Cu	29	64	85	49	14	1
Mn	770	772	901	769	1230	2480
Mo	1	2	2	1	2	2
Ni	47	59	57	80	103	32
Pb	15	15	21	8	15	11
Zn	65	86	66	86	124	45
V	101	121	120	150	204	658
S	0.045	0.068	0.246	0.015	0.081	0.001

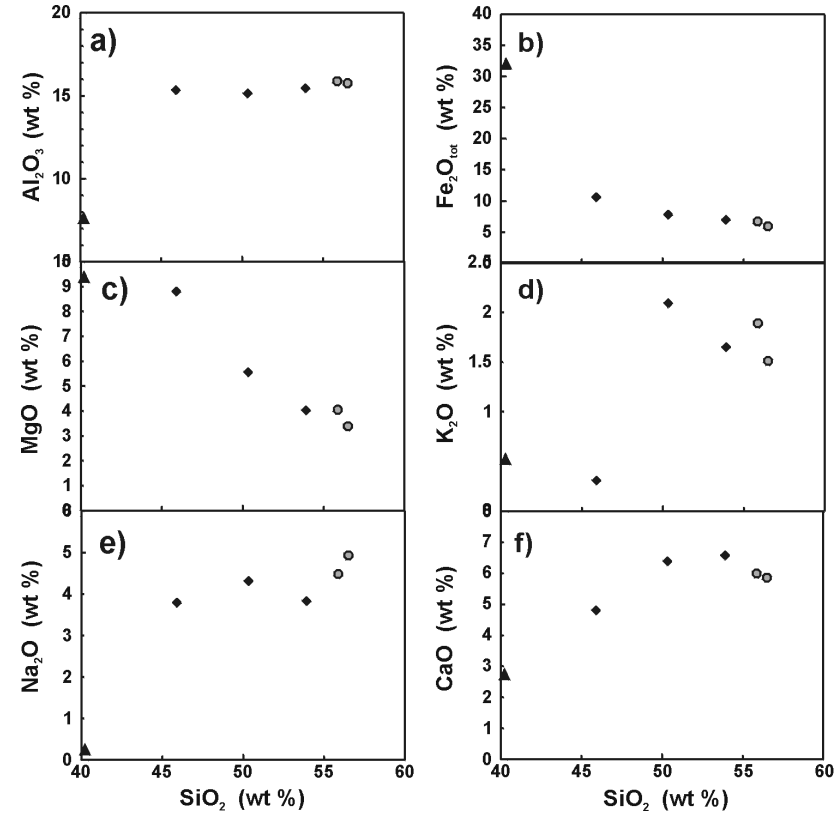

*Figure GS-15-3: SiO_2 versus a) Al_2O_3, b) $Fe_2O_{3\ tot}$, c) MgO, d) K_2O, e) Na_2O, and f) CaO in the granitoid samples (*see *Fig. GS-15-5 for symbols).*

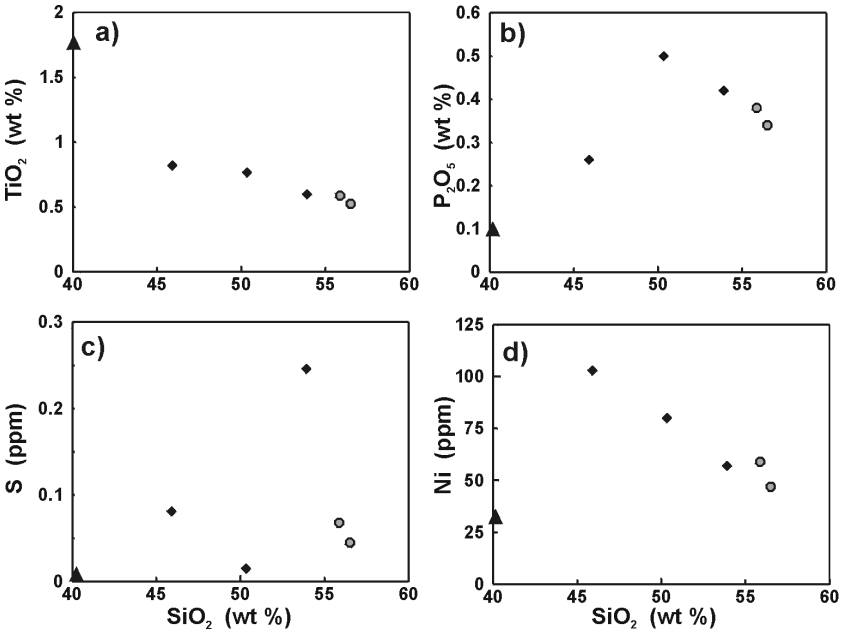

*Figure GS-15-4: SiO_2 versus a) TiO_2, b) P_2O_5, c) S, and d) Ni in the granitoid samples (*see *Fig. GS-15-5 for symbols).*

accompanied F_2 development and represents the most penetrative secondary fabric element.

Peck et al. (1998) interpreted the distribution of the iron-formation within the core of a shallow west-plunging anticlinorium (*see* Fig. GS-15-2). Key to this interpretation is the correlation of the dacite exposed along the south margin of the East pit and the rhyolite north of the pit as lateral facies equivalents. Consequently, the argillite exposed in the west wall of the East pit was interpreted to occupy the core of a shallowly west-plunging synform. Based on mesoscopic overprinting relationships, this fold is most likely a macroscopic F_1 fold. There is no systematic change in F_2 asymmetry across the argillite, suggesting that F_2 is not responsible for the distribution of the argillite and iron-formation.

The intensity of D_2 fabric development, demonstrating the partitioning of the deformation, is reflected in the large competency contrasts between the units that form the deposit stratigraphy. The iron-formation is tightly folded and moderately foliated. A steep D_2 strain gradient

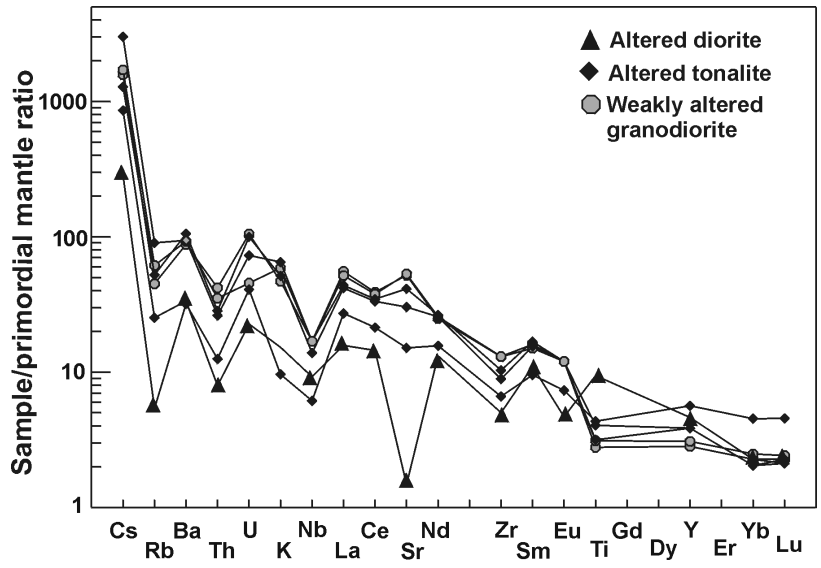

*Figure GS-15-5: Primitive-mantle–normalized spider diagram with the six samples illustrated (*see *Sun and McDonough, 1989 for normalizing values). The bolded elements are considered immobile under mostly hydrothermal alteration conditions.*

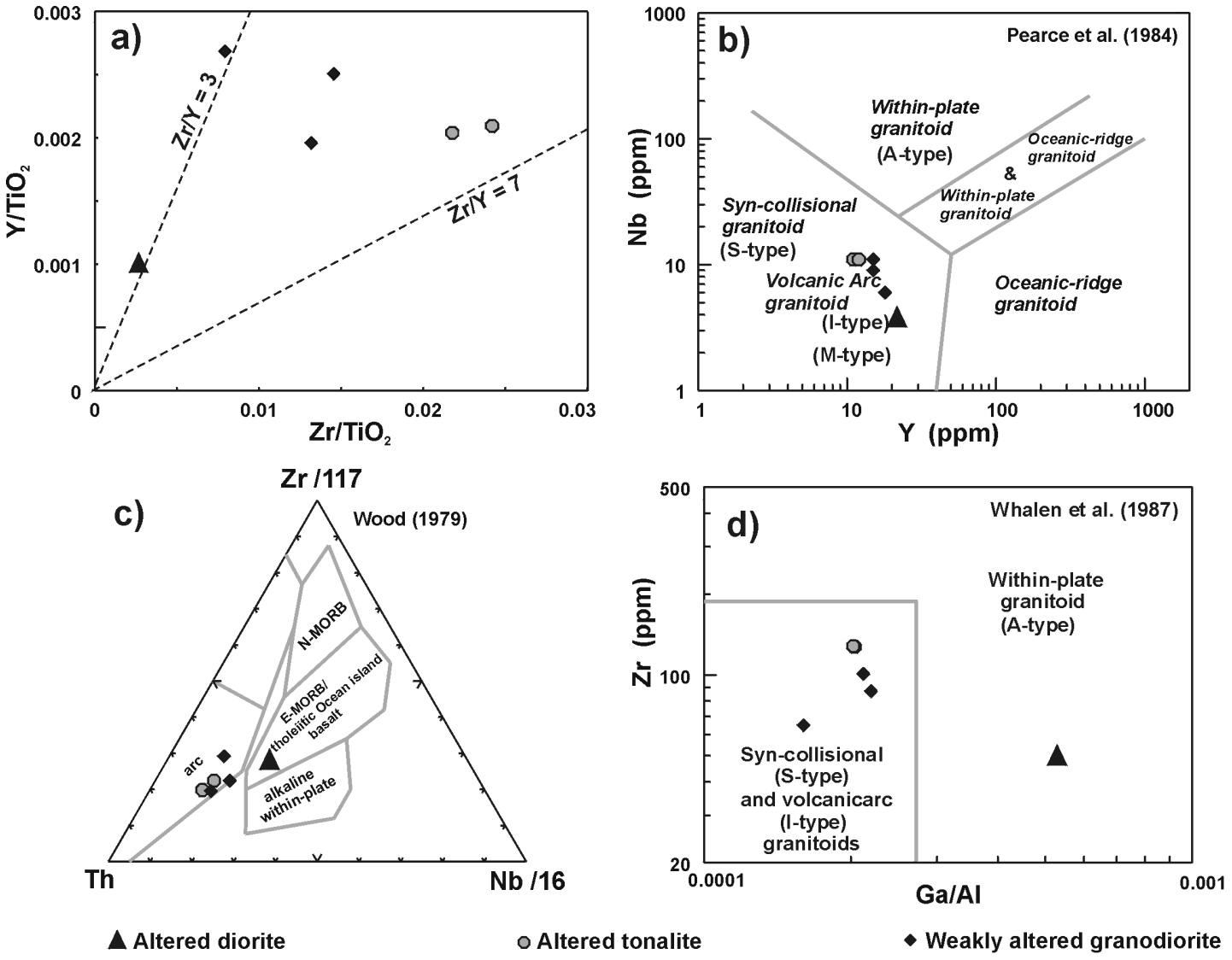

*Figure GS-15-6: a) Y/TiO_2 versus Zr/TiO_2 diagram, with Zr/Y illustrated, b) Nb versus Y discrimination diagram (*modified after *Pearce et al., 1984), c) Th-Zr-Nb discrimination diagram (*modified after *Wood, 1979); abbreviations: A, N-MORB affinity; B, E-MORB affinity; C, within-plate affinity; and D, volcanic-arc affinity, d) Zr versus Ga/Al (*see *Whalen et al., 1987).*

Figure GS-15-7: Steeply east-plunging F_2 fold in oxide-facies iron-formation.

along the southern contact between the iron-formation and the granodioritic intrusion is characterized by the development of protomylonite and a narrow zone of mylonitic fabrics in the iron-formation along the contact. The argillite interbedded with the iron-formation is intensely folded and foliated, as evidenced by the development of phyllitic zones and local fault displacement of F_2 limbs. The margin of the intermediate pluton exposed in the south wall of the East pit contains moderate S_2 foliation development and preserves an older S_1 slaty cleavage. An S_3 foliation and F_4 folds are also developed in the granodiorite.

Overprinting F_2 are two generations of close to open folds. The F_3 generation comprises northeast-trending, steeply plunging, Z-asymmetrical folds. Although mesoscopic F_3 folds are rare, a penetrative S_3 crenulation cleavage overprints older fabric elements. The youngest generation of folds comprises north- to northwest-trending, open chevron folds. Folds of the F_4 generation generally lack an axial-planar foliation, but produced small-scale tight crenulations, which locally have differentiated limbs that approximate a foliation.

Emplacement of the intermediate dykes postdates F_2 folding. The orientation of the dykes is subparallel to F_2 axial planes and the dykes do not outline any F_2 folds or boudinage. The dykes predate F_3 and generally contain an S_3-parallel spaced fracture cleavage. The intermediate intrusion (granodiorite to diorite) of the Pool Lake suite seems to intrude during late F_2 or early F_3.

Numerous premineralization faults transect the East pit. Many of these occupy F_2 limbs and appear to represent adjustments in response to the tight F_2 folding. Two major northwest-trending faults, the East and Wendy faults, postdate the folding events, since they transect F_2–F_4 axial traces. These parallel faults comprise steeply northeast dipping zones of intense fracturing cored by decimetre-scale gouge zones characterized by imbricated clasts, indicating a large component of normal movement.

GOLD METALLOGENY

Gold mineralization in the East pit is associated with two sets of centimetre- to decimetre-scale, coarse-grained, quartz-sulphide and quartz-dolomite-sulphide veins with minor chlorite (Fig. GS-15-8). The veins have a wide variety of textures, including open space, vuggy textures; laminated, crack-seal textures; and locally composite, zoned veins consisting of crack-seal textures along one side and sulphide-matrix quartz breccia along the other.

The timing of mineralization postdates both the folding and faulting events. There are numerous examples of mineralized flats transecting F_4 fold axes, the latest folding event, and both the Wendy and East faults (Fig. GS-15-9a, -9b). The shallow QSV (flats) were emplaced along shallowly southwest-dipping faults and joints. These brittle-ductile features record a sinistral offset of approximately 1 m. Narrow zones of sinistral ductile bending of the bedding laminations indicate the initiation of the joints as ductile structures followed by brittle failure due to the elevation of the strain rate. The subvertical QSV (steeps) were emplaced along moderate to steep south-southwest-dipping joints, along subvertical S_2 parallel faults, and within zones of intense S_2 foliation development (phyllitic zones). These mineralized veins are very high grade (approx. 30 g/t Au; Peck et al., 1998) and are mantled by zones (up

Figure GS-15-8: Shallowly southeast-dipping (flat) quartz-carbonate-sulphide vein. Note the sulphidic halo developed where the vein intersects iron–formation, and the slight ductile bending of the bedding lamellae adjacent to the vein.

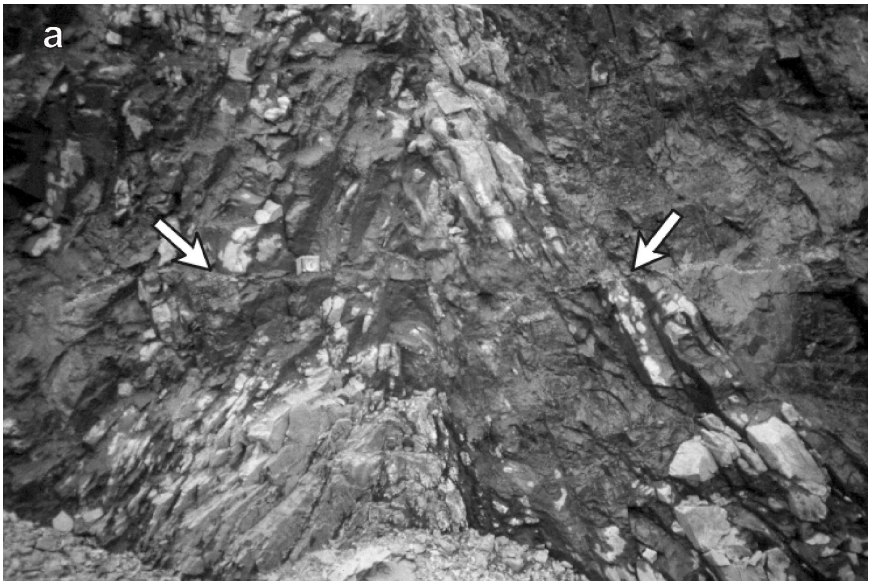

Figure GS-15-9: a) Emplacement of quartz-sulphide vein (QSV) following F_4 folding (arrow); b) QSV 'flat' emplacement following faulting (arrow).

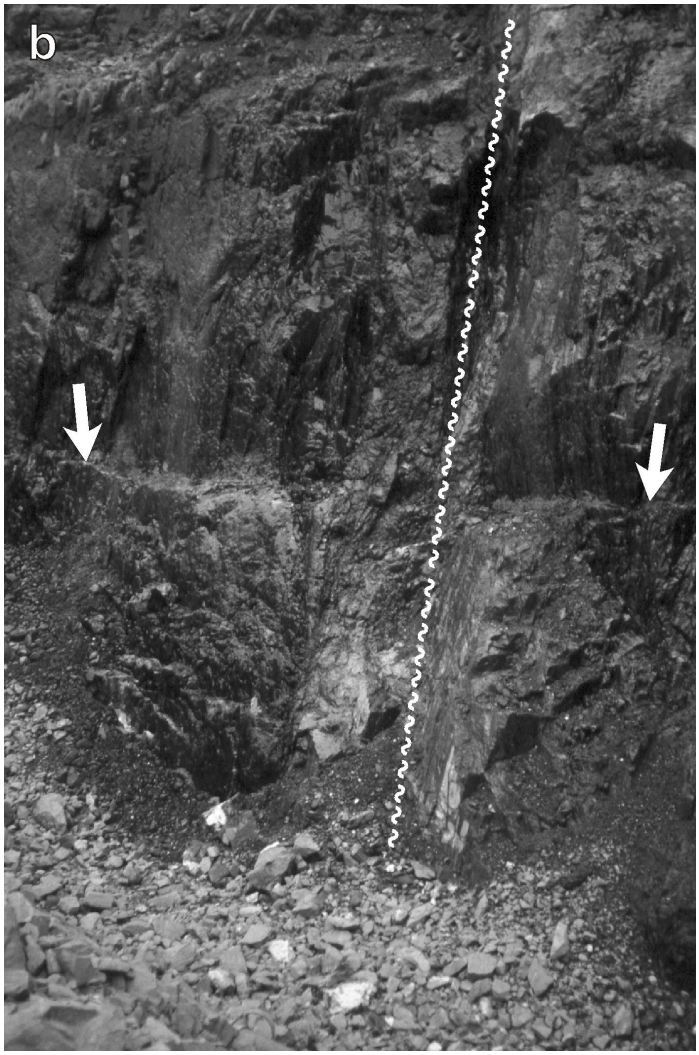

to 60 cm wide) of intense sulphidization of the host iron-formation. In the East pit, the sulphidization is manifested as replacement of the magnetite lamellae by pyrite (and gold), preserving the primary laminations and secondary foliations. The sulphidization halos are developed around both the steeps and the flats. The link between emplacement of the mineralization halos and sulphidization of magnetite is demonstrated by the lack of halo development where the QSV cut the interbedded argillite or intermediate dykes.

The low-temperature alteration assemblages in the later fabrics in all phases of the intrusions indicate that gold mineralization entirely postdates all intrusive events. As such, the gold is not associated with magmatic-hydrothermal activity related to these intrusive phases. It is possible that the late fabrics formed preferentially along the intrusion's north margin, which is the southern margin of the iron-formation–hosted gold mineralization and the focus of gold-mineralizing hydrothermal-fluid flow in the region; this could be due to the competency contrast between the iron-formation and the intrusion. Although this is consistent with the orientation of the southwest-dipping mineralized flats (faults/shears) and S_2 parallel steeps (phyllonite zones) in the area, the intermittent gold mineralization along the intrusive contact is not entirely consistent with this scenario, although the obvious control of sulphidization processes by magnetite may explain the minimal mineralization evident in the intermediate intrusion.

CONCLUSIONS

The intermediate Pool Lake suite intrusion is a zoned or composite intrusion with a massive granodioritic core grading to a marginal phase of dioritic composition. Although difficult to ascertain due to the variability of alteration, the granodioritic and tonalitic phases have a metaluminous volcanic-arc (I-type) affinity, whereas the diorite seems to have an Fe-rich tholeiitic character, possibly related to a first-phase extensional event associated with intrusion emplacement. The increase in fabric development and at least two stages of hydrothermal alteration (high T and low T) are recognized petrographically and seem to characterize the zone. An earlier foliation (S_2) in the outer margin, coupled with the generally discordant nature of the intrusion, suggests that it was emplaced syn- to post-F_2 folding and fabric development, which is consistent with the peak metamorphic mineralogy. Analogous to the late controls on gold-sulphide-quartz veining in the iron-formation–hosted sequence, the late chlorite-quartz-sulphide veins that locally contain gold in the intrusion are associated with faults and shears that seem to exploit the earlier S_2 fabric and related structures. As outlined before and based on fabric overprinting relationships, the gold mineralization is controlled by late brittle shears/joints that parallel the steep S_1-S_2 fabrics (steeps) and shallowly southwest-dipping brittle-ductile faults (flats) in the iron-formation and argillite. It is possible, especially considering the intensity of late shearing and low-temperature alteration along the intrusion-supracrustal contact, that the faulting and shearing were controlled, in part, by the competency contrast between the iron-formation and the altered intrusion margin. Although it does not seem that the intrusion played a direct role in the mineralizing process, it is probable that late auriferous hydrothermal solutions were focused from depth by these

structures and enhanced fabrics. Due to the selective nature of the sulphidization process (mainly of magnetite) that seems to be directly linked to mineralization, the intermediate intrusion was a less favourable host to the mineralization.

ACKNOWLEDGMENTS

This research is supported by the Manitoba Geological Survey, a grant from the Geological Survey of Canada and a grant from the University of New Brunswick. Additional in-kind support from Black Hawk Mining Inc. and their staff was invaluable to our research.Particular thanks are due to Paul Pawliw for his assistance. The manuscript was kindly reviewed by Mark Fedikow (MGS).

REFERENCES

Bateman, J.D. 1945: McVeigh Lake area, Manitoba; Geological Survey of Canada, Paper 45-14, 34 p.

Fedikow, M.A.F. 1995: Multi-media geochemical surveys at the Farley Lake gold deposits, Agassiz metallotect, Lynn Lake area, part 1: element distribution in the host rocks to the Wendy zone; Manitoba Energy and Mines, Geological Services, Economic Geology Report ER95-1, 32 p.

Fedikow, M.A.F. and Gale, G.H. 1982: Mineral deposit studies in the Lynn Lake area: *in* Report of Field Activities 1982, Manitoba Energy and Mines, Geological Services, p. 44–54.

Gilbert, H.P., Syme, E.C. and Zwanzig, H.V. 1980: Geology of the metavolcanic and volcaniclastic metasedimentary rocks in the Lynn Lake area; Manitoba Energy and Mines, Geological Services, Geological Paper GP80-1, 118 p.

Milligan, G.C. 1960: Geology of the Lynn Lake district; Manitoba Mines and Natural Resources, Mines Branch Publication 57-1, 317 p.

Pearce, J.A., Harris, N.B. and Tindle, A.G. 1984: Trace element discrimination diagrams for the tectonic interpretation of granitic rocks; Journal of Petrology, v. 25, p. 956–983.

Peck, D.C., Lin, S., Atkin, K. and Eastwood, A.M. 1998: Reconnaissance structural studies of the Au metallotects in the Lynn Lake greenstone belt (parts of NTS 64C/10, C/11, C/15); *in* Report of Activities 1998, Manitoba Energy and Mines, Geological Services, p. 69–74.

Richardson, D.J. and Ostry, G. 1996: Gold deposits of Manitoba; Manitoba Energy and Mines, Geological Services, Economic Report ER 86-1, 114 p. (second edition).

Sun, S.S. and McDonough, W.F. 1989: Chemical and isotopic systematics of oceanic basalts: implications for mantle composition and process; *in* Magmatism in the Ocean Basins; Geological Society, Special Publication 42, p. 313–345.

Whalen, J.B., Currie, K.L. and Chappell, B.W. 1987: A-type granites: geochemical characteristics, discrimination and petrogenesis; Contributions to Mineralogy and Petrology, v. 95, p. 407–419.

Winchester, J.A. and Floyd, P.A. 1977: Geochemical discrimination of different magma series and their differentiation products using immobile elements; Chemical Geology, v. 20, p. 325–343.

Wood, D.A., Joron, J-L. and Treuil, M. 1979: A re-appraisal of the use of trace elements to classify and discriminate between magma series erupted in different tectonic settings; Earth and Planetary Science Letters, v. 45, p. 326-336.